AIAA JOURNAL
Vol. 49, No. 7, July 2011

Hypervelocity Experiments on Oxygen Enrichment in a Hydrogen-Fueled Scramjet

Sarah A. Razzaqi* and Michael K. Smart†
University of Queensland, Brisbane, Queensland 4072, Australia

DOI: 10.2514/1.J050866

Extension of scramjet operation into the hypervelocity regime ($u > 3$ km/s, $M > 10$) is critical for their use in access-to-space systems. As flight speeds increase, the net thrust of a scramjet engine is limited by increased fuel/air mixing length requirements, as well as the decreased ratio of energy available from stoichiometric fuel/air combustion relative to the specific kinetic energy of the captured air. One possible method for addressing these issues, known as oxygen enrichment, involves the premixing of oxygen with fuel before injection. This method provides a head start for mixing and also allows the possibility of fuel combustion at greater than stoichiometric proportions. This paper describes some exploratory shock tunnel experiments involving oxygen enrichment of gaseous hydrogen fuel in a scramjet at hypervelocity conditions. These experiments were conducted in a simple rectangular duct with a central strut injector and varying levels of enrichment. The measured pressure distributions show a positive effect of enrichment and indicate how this technique could be best used to extend the performance of hypervelocity scramjets to higher flight Mach number.

Nomenclature

c_f	=	coefficient of friction
EP	=	enrichment percentage, %
F	=	thrust, N
F_{spec}	=	specific thrust, $F/\dot{m}_{\text{air}}$, Ns/kg
f	=	fuel-to-air ratio
f_{stoich}	=	stoichiometric fuel-to-air ratio
g	=	acceleration due to gravity, m/s
H	=	total enthalpy, MJ/kg
h	=	combustor height, 47 mm
I_{sp}	=	specific impulse, $F/[(\dot{m}_{\text{fuel}} + \dot{m}_{\text{oxy}})g]$, s
L	=	combustor length, 866 mm
M	=	Mach number
$\dot{m}_{\text{air}}$	=	mass flow rate of air, kg/s
$\dot{m}_{\text{fuel}}$	=	mass flow rate of fuel, kg/s
$\dot{m}_{\text{nit}}$	=	mass flow rate of premixed nitrogen, kg/s
$\dot{m}_{\text{oxy}}$	=	mass flow rate of premixed oxygen, kg/s
p	=	static pressure, kPa
p_c	=	combustor entrance pressure, kPa
p_{norm}	=	normalized pressure
p_s	=	nozzle-supply pressure, MPa
q	=	dynamic pressure, kPa
T	=	static temperature, K
u	=	velocity, m/s
u_e	=	engine exit velocity, m/s
u_0	=	flight velocity, m/s
W	=	combustor width, 100 mm
X	=	length-scale measure in combustion efficiency curve
x	=	axial position, mm
x_{end}	=	axial position of end of combustor, mm
x_{ig}	=	axial position of ignition, mm
y	=	transverse position, mm
η_c	=	combustion efficiency, $\eta_{c,e}[\theta X/(1 + (\theta - 1)X)]$, %
$\eta_{c,e}$	=	combustion efficiency at end of combustor, %
θ	=	empirical constant to determine slope of combustion efficiency curve
ρ	=	density, kg/m^3
ϕ	=	equivalence ratio
ϕ_{eff}	=	effective equivalence ratio

I. Introduction

IN THE continuing effort to achieve more affordable access to space, scramjets have been considered for use in multistage launch vehicles because of their high specific impulse relative to rockets. For these next-generation launch vehicles to be useful, the scramjet stage should be able to operate in the hypervelocity regime, i.e., at velocities greater than 3 km/s and Mach numbers in excess of 10. In addition, the ability to operate over a wide range of Mach numbers is essential for an accelerating system [1–3]. As a scramjet vehicle travels along a typical constant dynamic pressure trajectory to higher altitudes and Mach numbers it becomes increasingly difficult to generate enough thrust to overcome the drag of the vehicle. The reasons for this are twofold. First, as flight speeds increase, so does the velocity of the air that passes through the engine (typically ~85–95% of flight velocity). Increased combustor air velocity leads to longer lengths for adequate mixing of fuel and air and the need for longer combustors. However, longer combustors result in increased internal drag and heat loads, so in most instances it is not practical to operate high-speed scramjets near stoichiometric combustion levels. Many injection/mixing schemes have been developed in response to this issue [4–6]. Second, the energy available from hydrogen fuel combustion becomes a smaller proportion of the kinetic energy per unit mass of the airstream as flight speeds increase. For example, the typical energy available from hydrogen or hydrocarbon fuels at stoichiometric proportions is ~3.45 MJ/kg of air. At a flight speed of 2 km/s (Mach number ~6), this corresponds to approximately 1.7 times the freestream kinetic energy per unit mass, so efficient conversion of this chemical energy to increased velocity of the combustion products exiting the engine results in high engine thrust. At a flight speed of 2.6 km/s the available chemical energy and the flight kinetic energy per unit mass are approximately equal, and at a flight speed of 3 km/s this ratio reduces to 0.77. Efficient conversion of chemical energy to thrust becomes more and more critical as flight speed increases. It is clear

Presented at the 16th AIAA/DLR/DGLR International Space Planes and Hypersonic Systems and Technologies Conference, Bremen, Germany, 19–22 October 2009; received 16 August 2010; revision received 20 December 2010; accepted for publication 20 January 2011. Copyright © 2011 by S. A. Razzaqi and M. K. Smart. Published by the American Institute of Aeronautics and Astronautics, Inc., with permission. Copies of this paper may be made for personal or internal use, on condition that the copier pay the $10.00 per-copy fee to the Copyright Clearance Center, Inc., 222 Rosewood Drive, Danvers, MA 01923; include the code 0001-1452/11 and $10.00 in correspondence with the CCC.

*Ph.D. Candidate, Centre for Hypersonics, School of Mechanical and Mining Engineering. Student Member AIAA.

†Professor, Centre for Hypersonics, School of Mechanical and Mining Engineering. Senior Member AIAA.

from this discussion that the possibilities for scramjet thrust generation diminish as we enter the hypervelocity regime.

To examine the generation of scramjet thrust it is instructive to consider the thrust equation for an airbreathing engine. When it is assumed the exit flow is fully expanded, the uninstalled thrust is given by

$$F = \dot{m}_{\text{air}} u_0 \left[(1+f)\frac{u_e}{u_0} - 1 \right] \tag{1}$$

where u_0 is the flight velocity, $\dot{m}_{\text{air}}$ is the mass flow rate of air captured by the engine, $f = \dot{m}_{\text{fuel}}/\dot{m}_{\text{air}}$ and u_e is the velocity of the air/combustion products leaving the engine. Thrust is generated first and foremost by increasing u_e through combustion of fuel and air up to stoichiometric proportions ($f = f_{\text{stoich}}$). However, Eq. (1) makes it clear that increasing the fuel mass flow rate also has a direct effect on thrust. Fuel injection at rates above stoichiometric (or injection of other fluids) can be used to increase thrust. A cycle analysis based study of this effect by Rudakov and Krjutchenko [7], involving a hydrogen-fueled scramjet examined from Mach 8 to 20, indicated injection of hydrogen at greater than stoichiometric proportions increased thrust, but at reduced specific impulse. The injection of heavy inert species such as neon and argon showed similar characteristics. This same study also considered the idea of not only injecting excess hydrogen, but combining it with injection of oxygen that can then combust with the extra fuel. This idea, known as *oxygen enrichment*, was found to generate increased thrust while maintaining specific impulse, despite the significantly increased fuel/oxidizer flow rates. A later system study by Pike [8] confirmed these results, indicating that from a cycle perspective, oxygen enrichment can generate the extra thrust needed at high Mach number with little degradation of specific impulse. Note that this idea is different from operating a fuel-rich rocket in a scramjet duct, know as a rocket-based combined-cycle engine, which does suffer a significant penalty in specific impulse [9].

Given the promising theoretical performance of oxygen enrichment, it is somewhat surprising that detailed experiments have not been performed to date. In an effort to fill this gap, a set of exploratory experiments were conducted at the University of Queensland in the T4 shock tunnel. For this study, significant efforts were made to experimentally measure the effect of oxygen enrichment in a geometrically simple scramjet. To this end, the flowpath involved a semi-direct-connect experiment with relatively uniform hypervelocity flow entering a constant-area rectangular combustor. Gaseous hydrogen fuel was injected from a 2-D central strut on the centerline of the duct, and tests were performed with and without gaseous oxygen that was premixed with the fuel before injection. This paper first describes the model and test conditions, followed by a description of the fuel delivery and mixing system used in the experiments. A brief description is given of the cycle analysis code used in this study. The experimental results are then presented, largely in the form of pressure distributions along the combustor, followed by some discussion and conclusions.

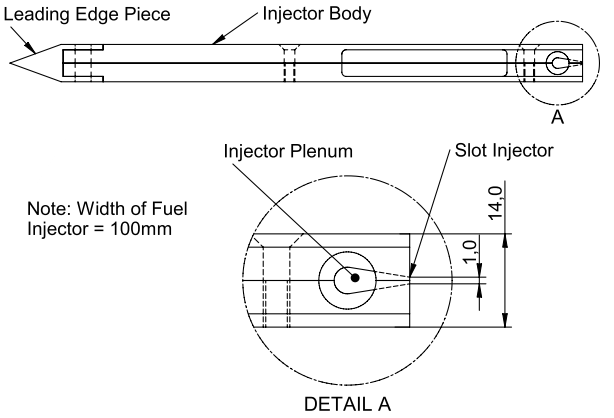

Fig. 2 Detail view of fuel injector. Dimensions are in millimeters.

II. Experimental Model and Instrumentation

The model used for these experiments consisted of a two-dimensional intake, a long constant-area rectangular combustor ($L/h = 18.4$, $W/h = 2.1$), a central strut injector, and a short expansion nozzle with an area ratio of 3.3. A cross section of the assembled model is shown in Fig. 1. The 2-D intake consisted of 8° wedges with parallel side walls that compress the flow exiting the facility nozzle to the conditions desired at the entrance to the combustor. This intake had a compression ratio of 6.4 at the approximately Mach 6 flow exiting the facility nozzle and was immediately followed by spillage holes that allowed the intake boundary layers and shocks to be expelled. The centrally mounted fuel injector strut also produced shocks and expansion waves that processed the flow entering the combustor, and its leading edge was set upstream of the combustor entrance so that these waves were also expelled via the spillage holes. Fuel injection was through a 1 mm slot in the base of the injector strut that spanned the width of the combustor. Figure 2 shows some close-up detail and dimensions of the sonic fuel injector and plenum, showing that the injector slot filled 7% of the base area of the strut.

The model was instrumented with pressure transducers of two different types. The lower wall of the combustor was instrumented with piezoresistive pressure transducers (Kulite Semiconductor Products, Inc.) at 40 mm spacing along the centerline. The expansion surface was instrumented with piezoelectric pressure transducers (PCB Piezotronics, Inc.) for the most part at 20 mm spacing along the centerline. In addition, the lower intake wedge and the intake sidewalls were instrumented with PCB pressure transducers.

III. Test Facility and Conditions

The experiments were carried out in The University of Queensland's T4 free-piston reflected-shock tunnel [10]. The facility has a 229-mm-diam driver that is 26 m in length and a 75-mm-diam shock tube that is 10 m in length. A series of contoured axisymmetric nozzles are available for use over a wide range of

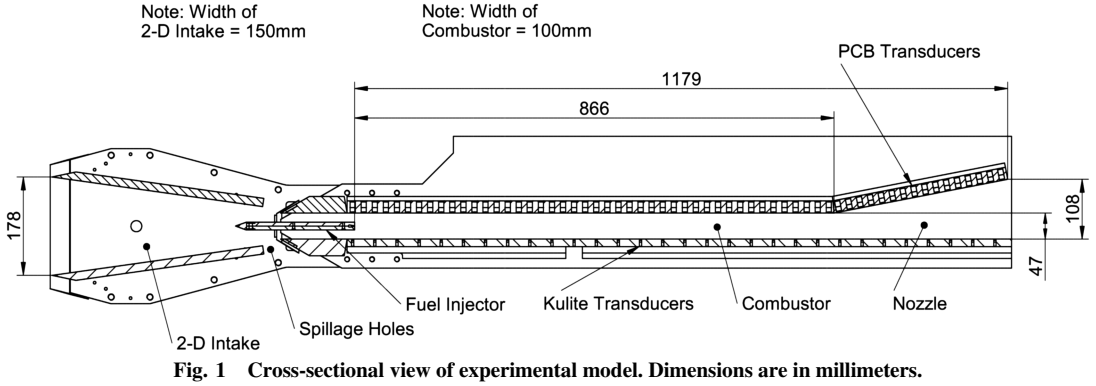

Fig. 1 Cross-sectional view of experimental model. Dimensions are in millimeters.

hypervelocity conditions of interest to scramjet designers. A Mach 6 nozzle with a throat diameter of 25 mm and an exit diameter of 262 mm (area ratio of 10.5) was used for these experiments to achieve the desired conditions entering the model. A pitot-rake survey was initially performed to characterize the nozzle flow at the entrance of the model. Figure 3 shows the contours of experimental pitot pressure normalized by nozzle-supply pressure at this station, with the capture area of the 2-D intake and the combustor entrance superimposed. As the figure shows, the flow entering the model is relatively uniform, except at the corners of the 2-D intake. These corner flows, along with the boundary layers that build up in the intake, are intended to be bled off before the flow enters the combustor (which has a smaller width than the intake). A pitot-to-nozzle-supply pressure ratio of 0.015 was used to calculate the flow conditions entering the combustor in the current experiments.

Typical time histories for nozzle-supply pressure and a typical model static pressure are shown in Fig. 4, with a time offset of 330 μs applied to the latter signal to account for the time taken for the flow to travel from one measurement location to another and with $t = 0$ at the onset of flow. Experimental and numerical studies have been conducted to determine flow establishment times [11] as well as to determine when driver gas contamination occurs [12] for the facility. For the conditions of these experiments, flow establishment takes approximately 1.2 ms and the test time is approximately 0.8 ms. The nominal mass capture of the engine model was 0.77 kg/s.

It was desired to perform experiments simulating flight at a Mach number near 12 and a dynamic pressure close to 50 kPa. As the model being tested was not a complete engine, a representative engine was chosen in order to estimate the equivalent flight conditions corresponding to the experiments. This representative engine was taken to be a rectangular-to-elliptical shape-transition engine designed for flight at Mach 12 [13]. Table 1 lists all the relevant flow parameters, with the first two columns containing the facility nozzle exit and combustor entrance conditions achieved in the experiments and the last column containing the equivalent flight conditions. These values indicate that the flight Mach number is slightly higher than desired, but flight dynamic pressure falls short by approximately 20%. Note that flight at Mach 12.3 and a dynamic pressure of 40.2 kPa corresponds to an altitude of 37.7 km.

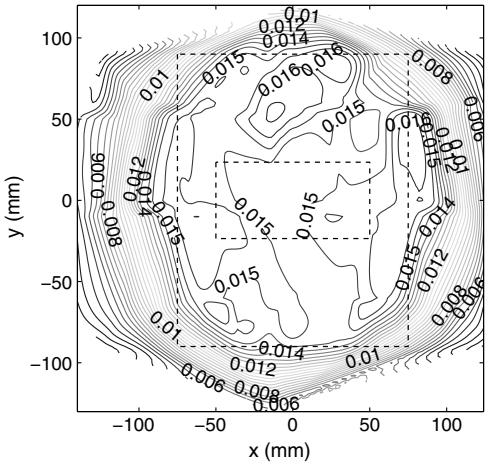

Fig. 3 Contours of pitot-to-nozzle-supply pressure ratio. Capture area of 2-D intake and combustor indicated by dashed lines.

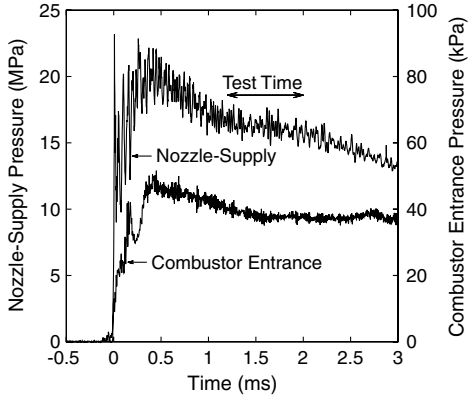

Fig. 4 Typical nozzle-supply and combustor entrance pressures during an experiment.

IV. Fuel/Oxidizer Delivery and Mixing System

The amount of fuel injected and the level of enrichment in an experiment are quantified by the fuel equivalence ratio and similar expressions to describe the level of oxygen enrichment. The equivalence ratio is defined as

$$\phi = \frac{f}{f_{\text{stoich}}} \tag{2}$$

where f is the actual ratio of fuel to air, and f_{stoich} is the stoichiometric ratio of fuel to air. Considering a simplified hydrogen–oxygen reaction, 1 mol of oxygen is required to completely consume two moles of hydrogen. Converting to units of mass, this means that 32 g of oxygen are needed to consume 4 g of hydrogen; i.e., the mass of oxygen should be eight times that of hydrogen in a stoichiometric reaction. Assuming standard air with an oxygen percentage of 23.2%, the equivalence ratio for the hydrogen-air reaction is then given by

$$\phi = 8\frac{\dot{m}_{\text{fuel}}}{0.232\dot{m}_{\text{air}}} \tag{3}$$

Note that the equivalence ratio relates the mass flow rate of injected fuel to the mass flow rate of air entering the combustor. It is not affected by additional oxygen from enrichment. However, it is instructive to also consider an effective equivalence ratio, which does include the premixed oxygen. In this paper, effective equivalence ratio is defined as

$$\phi_{\text{eff}} = 8\frac{\dot{m}_{\text{fuel}}}{0.232\dot{m}_{\text{air}} + \dot{m}_{\text{oxy}}} \tag{4}$$

The effective equivalence ratio does not provide enough information to compare the relative amount of freestream oxygen to premixed oxygen between different experiments. For this purpose, a parameter termed the enrichment percentage (EP) is used and is defined for hydrogen fuel as

$$\text{EP} = \frac{1}{8}\frac{\dot{m}_{\text{oxy}}}{\dot{m}_{\text{fuel}}} \times 100 \tag{5}$$

In other words, the enrichment percentage is the percentage of fuel that can be burnt (assuming complete combustion) by the premixed oxygen. As an example, if the mass flow rate of the additional oxygen is twice that of hydrogen, then EP = 25; i.e., 25% of the hydrogen is able to react with the premixed oxygen while the remaining 75% must mix and burn with the oxygen in the combustor airflow. The enrichment percentage is not related to the combustor airflow in any way, rather it is a measure of how much of a head start to mixing is provided by enrichment. Note also that an EP = 25 at $\phi = 1.0$

Table 1 Test conditions and equivalent flight conditions

	Facility nozzle exit condition	Combustor entrance condition	Equivalent flight condition
H, MJ/kg	7.6	7.6	7.6
M	5.7	3.8	12.3
T, K	976	1860	244
p, kPa	6.19	39.57	0.38
ρ, kg/m^3	0.022	0.073	0.005
u, m/s	3510	3187	3845
q, kPa	135.5	370.7	40.2

involves the addition of twice as much oxygen as EP = 25 at $\phi = 0.5$ given the same engine mass capture.

The T4 fuel/oxidizer delivery and mixing system stores fuel and oxidizer separately at room temperature before a test, initiates the flow of fuel and oxidizer upon commencement of a test, mixes the fuel and oxidizer, and finally injects the mixture into the combustor. It is made up of four major subsystems; the fuel delivery system, the oxidizer delivery system, the mixing system, and the fuel injector. The oxidizer delivery system and the mixing system were designed by Portwood [14] for use in a previous set of experiments. They are designed in accordance with ASTM International guidelines regarding oxygen-rich systems. For additional safety, a diluted oxidizer (75% oxygen, 25% nitrogen) was used for these experiments.

Both the fuel and oxidizer delivery systems employ a Ludwieg tube to supply gas at constant pressure and temperature for a duration sufficient for testing in T4. Long lengths of coiled tube (10 m+) are used for the Ludwieg tubes, and fast-acting solenoid valves act as diaphragms between the reservoirs (i.e., the Ludwieg tubes) and the mixing system. A schematic of the complete system is shown in Fig. 5. The majority of each Ludwieg tube is located outside the T4 test section, with short sections of tube inside the test section to connect to the solenoid valves. The valves and the mixing system are located next to the scramjet model, and the fuel injector is in the model strut (Fig. 1). A photograph of the solenoid valves and mixing system hardware is shown in Fig. 6.

Upon receiving an initiation trigger from the tunnel, the fast-acting solenoid valves are opened to allow fuel and oxidizer to flow from their respective Ludwieg tubes into their respective premix chambers. Fuel and oxidizer then flow into the mixing chamber through small orifices, where they are presumed to fully mix. From the mixing chamber the fuel/oxidizer mixture is piped to the injector plenum chamber, and finally the mixture passes through the injection slot into the combustor. It is intended that both fuel and oxidizer are choked upon entering the mixing chamber and that the fuel/oxidizer mixture is choked upon entering the injector plenum. The fuel/oxidizer mixture is then injected into the combustor at sonic conditions. Choking the fuel and oxidizer flow upon entering the mixing chamber is necessary in order to measure their individual mass flow rates. As a backup, the fuel/oxidizer mixture flow rate can be measured at the choke point entering the injector plenum. As will be seen, this redundancy was needed to determine the proportions of fuel and oxidizer used in the experiments. The fuel and oxidizer premix chambers, the mixing chamber and the injector plenum chamber were all fitted with PCB pressure transducers to measure each time history.

Figure 7 shows time histories of all the chamber pressures during a typical experiment, along with the T4 nozzle-supply pressure to indicate the timing of the test flow. Note that the time scales of the fuel/oxidizer system operation are an order of magnitude longer than the test flow duration. The key requirement on the fuel/oxidizer system is therefore to supply constant flow rates during the very short test time. To facilitate this, the fuel/oxidizer system was initiated approximately 40 ms before the test flow. The fuel premix chamber reaches steady state after approximately 15 ms, but experiences a dip in fuel pressure at 30 ms as a result of the expansion from opening the

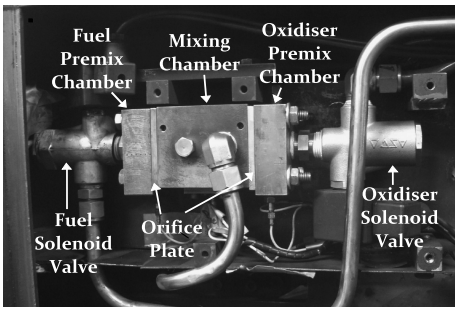

Fig. 6 Fuel/oxygen mixing system as mounted in test section.

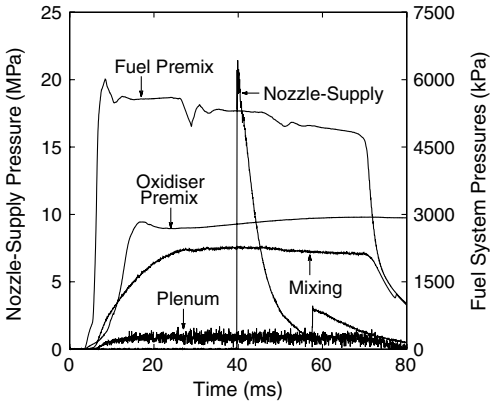

Fig. 7 Typical fuel premix chamber, oxidizer premix chamber, mixing chamber, injector plenum, and nozzle-supply pressures during an experiment.

solenoid valve passing through the Ludwieg tube, reflecting off the closed end, and arriving back at the premix chamber. However, at 40 ms when the test time occurs, the fuel premix pressure is again steady, but slightly lower. The oxidizer premix chamber reaches a steady state value at 30 ms and rises slowly thereafter. No dip is observed in this instance due to the significantly lower sound speed in the oxidizer. The mixing chamber takes some time to reach steady state due to its large volume, but is steady by the time the test flow occurs. Unfortunately, the injector plenum chamber signal was very noisy through all experiments (as indicated in Fig. 7); however, its mean value does appear steady during the test period.

A pressure drop by a factor of 2 between components in a gas flow system generally indicates choked flow between components. From Fig. 7 it is therefore clear that the fuel flow into the mixing chamber is choked (as desired), flow between the mixing chamber and the injector plenum is choked (as desired), whereas oxidizer flow into the mixing chamber is not (not as desired). Given this, an iterative procedure was used to determine the individual flow rates of fuel and oxidizer, as the relative fractions of fuel and oxidizer were needed to determine the mass flow rate of the mixture entering the injector plenum. Note that the fuel injector plenum pressure was not needed to determine these flow rates.

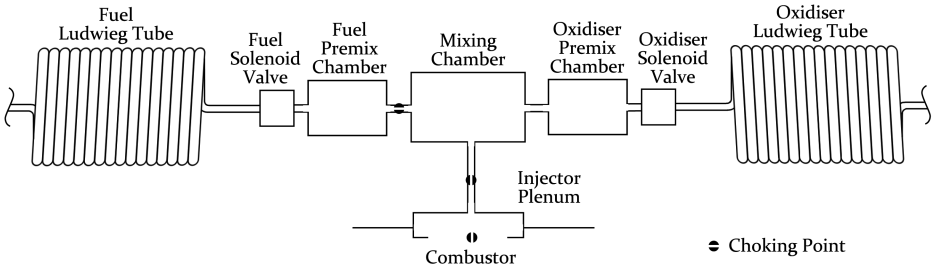

Fig. 5 Schematic of complete fuel/oxygen system. Adapted from Portwood [14].

Table 2 Fuel/oxidizer conditions

Description	ϕ	ϕ_{eff}	EP, %	$\dot{m}_{\text{fuel}}$, kg/s	$\dot{m}_{\text{oxy}}$, kg/s	$\dot{m}_{\text{nit}}$, kg/s
Fuel off	——	——	——	——	——	——
Suppressed combustion	1.03	1.03	——	0.023	——	——
Suppressed combustion	0.85	0.85	——	0.019	——	——
Fuel into air	0.84	0.84	——	0.019	——	——
Fuel into air	0.68	0.68	——	0.017	——	——
Fuel into air	1.01	1.01	——	0.023	——	——
Enriched	0.86	0.82	6.4	0.019	0.010	0.003
Enriched	0.81	0.72	13.9	0.018	0.020	0.007
Enriched	0.57	0.53	15.3	0.013	0.016	0.005
Enriched	0.98	0.87	12.4	0.021	0.021	0.007

V. Cycle Analysis

Analysis of combustion in the experimental model involved the use of quasi-one-dimensional cycle analysis methods. While the real combusting flow was far from uniform at any cross section, when used properly, these techniques provided an efficient means of determining the combustion efficiency in the duct. The cycle analysis code used [15] enabled prediction of the pressure distribution in the regions of the engine affected by combustion, therefore enabling comparison with experimental data. It was based on the classical gasdynamic methods presented by Shapiro [16], but with the flow modeled as a mixture of thermally perfect gases that are in thermal equilibrium. Skin-friction drag and heat transfer to the wall were estimated with a skin-friction coefficient of $c_f = 0.0025$ and use of Reynolds analogy. The area distribution of the combustor is an input to a cycle calculation, and the amount of fuel allowed to react at a particular station was dictated by a combustion efficiency curve. This combustion efficiency curve modeled both the mixing and kinetic aspects of the combustion and was adjusted to match the measured pressure distributions. Accurate knowledge of the mass flow rate, momentum flux, and specific total enthalpy of both the incoming air and fuel/oxidizer mixture are needed for meaningful results to be obtained. The key limitation of the code for the current application was the assumption of quasi-one-dimensional flow. The form of the combustion efficiency curve used here was taken from Heiser and Pratt [17] and contained two free parameters as follows:

$$\eta_c = \eta_{c,e} \frac{\theta X}{1 + (\theta - 1)X} \tag{6}$$

These are $\eta_{c,e}$, the combustion efficiency at the end of the combustor and θ, an empirical constant of order 1 to 10 which determines the initial slope of η_c at ignition. The length-scale measure is $X = (x - x_{ig})/(x_{\text{end}} - x_{ig})$.

VI. Results and Discussion

Four different types of tests were conducted to evaluate the impact of enrichment on the combustion behavior in the current scramjet model at hypervelocity conditions.

1) Fuel-off tests are experiments with no fuel injection and an air test gas to establish a baseline.

2) Suppressed-combustion tests use fuel injected into a nitrogen test gas to establish the level of pressure rise attributable to momentum/mass addition from injection.

3) Fuel-into-air tests use fuel injected into an air test gas to establish the level of pressure rise attributable to combustion (determined from comparison with the suppressed-combustion case).

4) Enriched tests use fuel premixed with oxidizer injected into an air test gas to determine the effects of oxygen enrichment on combustion.

Experiments were conducted at a variety of equivalence ratios and enrichment percentages, the results of which are shown as normalized pressure distributions along the combustor. To account for shot-to-shot variation, the data is presented as a normalized pressure of the form

$$p_{\text{norm}} = \frac{p}{p_s} \left(\frac{p_s}{p_c} \right)_{\text{standard}} \tag{7}$$

where p is the pressure measured at some location in the combustor, p_s is the measured facility nozzle-supply pressure for an experiment, and $(p_s/p_c)_{\text{standard}}$ is the standard nozzle supply to combustor entry pressure ratio for the test. A schematic of the model is included above the first pressure distribution to highlight the fuel injection location, indicate the start of the expansion nozzle, and show the most common arrangement of the pressure transducers (shown as solid

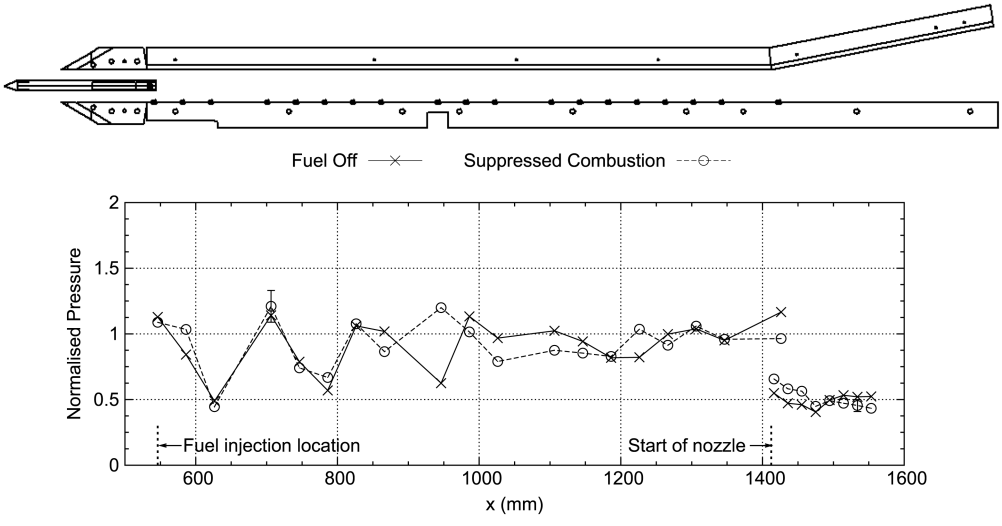

Fig. 8 Pressure distributions comparing fuel-off ($\phi = 0$, EP = 0) and suppressed combustion ($\phi = 1.03$, EP = 0).

black circles). Later figures omit this schematic, but do include a note on the location of fuel injection and the start of the nozzle. The fuel/oxidizer injection conditions for the presented results are summarized in Table 2.

To provide a baseline for the interpretation of fueled experiments, Fig. 8 shows the measured pressure distributions for both fuel-off and suppressed combustion at an equivalence ration of $\phi = 1.03$. The first pressure tap in the duct is slightly upstream of fuel injection, so both cases show a pressure close to the inflow level. A series of expansion waves are generated at the base of the injector strut, along with a recompression shock, and these waves dominate both fuel-off and suppressed-combustion plots. The initial expansion drops the measured pressure to approximately half the inflow pressure, but for both experiments, the following waves and the boundary-layer growth on the duct walls raise the pressure at the end of the duct to a level close to the inflow pressure. The main effect of fuel addition without combustion is to change the details of the wave structure in the duct, without any change in the overall pressure rise. The pressure on the nozzle expansion surface drops to approximately half the inflow pressure, which is consistent with a 2-D expansion fan. No influence of reflected expansion waves from the opposite flat surface was observed.

Figure 9 shows a pressure plot of fuel into air at $\phi = 0.84$, along with a suppressed combustion at $\phi = 0.85$ plot for comparison. The first thing to notice is that the fuel-into-air plot is very close to the suppressed-combustion plot until approximately $x = 900$ mm. This is 350 mm downstream of fuel injection ($\sim$7.5 duct heights). After this point, a clear difference was measured between suppressed combustion and fuel into air, which raised the pressure at the end of the duct to greater than 1.5 times the inflow pressure. This combustion generated pressure rise was also observed in the expansion nozzle. In addition to the experimental data, Fig. 9 shows a plot of the results of 1-D cycle analysis for the fuel-into-air case. This plot was generated using the code described earlier, with a combustion efficiency distribution shown in Fig. 10 (EP = 0). In the cycle analysis, fuel was added at the end of the strut ($x = 546$ mm) but was not allowed to start combusting until $x = 900$ mm. The parameters governing the distribution of combustion efficiency (θ and $\eta_{c,e}$) were chosen so as to match the measured pressure rise downstream of $x = 900$ mm. This indicated that the experimentally observed pressure rise corresponded to a combustion efficiency at the end of the duct of $\eta_{c,e} = 45\%$.

Results from fuel-into-air experiments at increasing equivalence ratio are shown in Fig. 11. It was observed that variation of ϕ between 0.68 and 1.00 had very little effect on the point of ignition, but did result in an increased pressure rise at the end of the duct and in the nozzle as ϕ increased. Pressure distributions generated by cycle analysis (not shown) indicated that increasing ϕ resulted in a decrease in the final combustion efficiency at the end of the duct. Hence increasing the fuel flow rate did not increase the proportion of captured oxygen that was mixed and combusted with the injected fuel. This characteristic suggests that combustion is mixing-limited and that fuel injection from the central strut reaches an effective mixing limit by the end of this very long duct; i.e., it only enables mixing with a proportion of the captured air.

Now that a set of results for fuel into air has been established, it is of interest to examine the effect of oxygen enrichment on the measured pressure distributions in the combustor duct. Figure 12 shows a comparison between suppressed combustion and fuel into air with oxygen enrichment at EP = 6.4. In this instance the fuel into air with enrichment shows a noticeable pressure rise (relative to suppressed combustion) at approximately $x = 830$ mm. This pressure rise reaches a value of 1.5 times the inflow pressure by $x = 1100$ mm ($x/h = 11.8$, relative to injection location), after which the pressure remains relatively constant. Comparing this with Fig. 9, which showed a comparison at the same ϕ but with no enrichment, it appears that enrichment has moved the point of ignition upstream (from $x = 900$ mm to $x = 830$ mm) and produced a similar peak pressure rise but at a much earlier position in the duct. Note that both Figs. 9 and 12 show results with the same amount of fuel mass flow. The only difference is that the enriched case included enough premixed oxygen to fully combust 6.4% of the fuel. This premixing has had two important effects at these hypervelocity conditions:

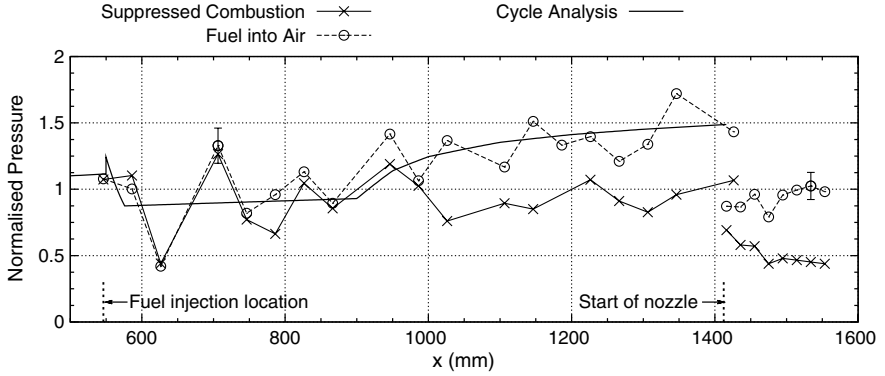

Fig. 9 Pressure distributions comparing fuel into air ($\phi = 0.84$, EP = 0) and suppressed combustion ($\phi = 0.85$, EP = 0).

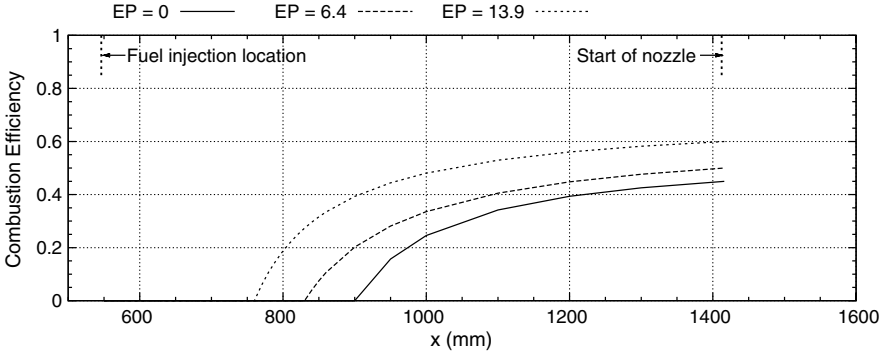

Fig. 10 Combustion efficiency curves used for cycle analysis of fuel into air with different enrichment levels at $\phi \sim 0.85$.

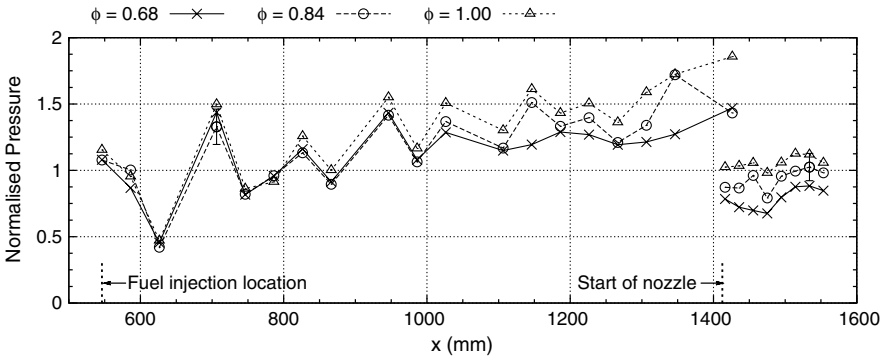

Fig. 11 Pressure distributions comparing fuel-into-air experiments at increasing equivalence ratio.

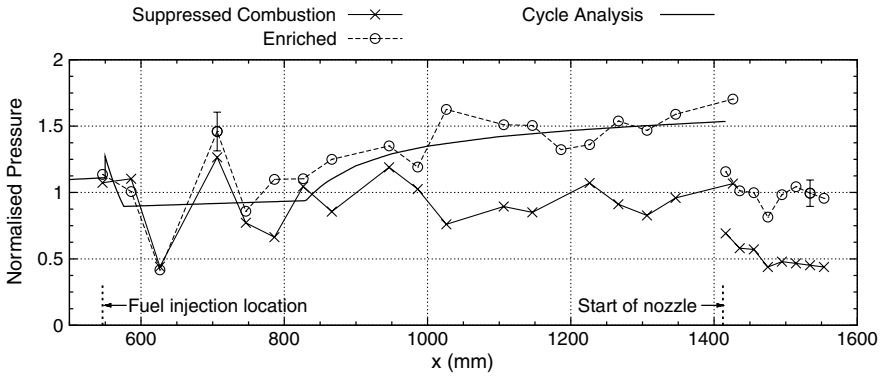

Fig. 12 Pressure distributions comparing enriched ($\phi = 0.86$, EP = 6.4) and suppressed combustion ($\phi = 0.85$, EP = 0).

1) It has shortened the ignition length for combustion.

2) It has shortened the duct length at which fuel injection from the strut reaches its effective mixing limit.

Figure 12 also shows the cycle analysis calculation that matches the experimental pressure rise for the enriched case. This pressure distribution was generated assuming a combustion efficiency curve plotted in Fig. 10 that had an ignition point at $x = 830$ mm and a combustion efficiency at the end of the duct of $\eta_{c,e} = 50\%$, i.e., greater than the no-enrichment case by an amount approximately equal to the level of premixing. So oxygen enrichment promotes ignition and adds to the overall mixing capability of the central strut by an amount similar to that of the premixing level.

Ignition is dependent on two factors; local equivalence ratio and chemical reaction rates. The latter are governed primarily by temperature and pressure and for supersonic combustion are estimated using the correlations established by Pergament [18]. The temperature of the flow is very high in these experiments, hence chemical reaction rates are high. Ignition is therefore dictated by the local equivalence ratio. For robust combustion to occur, the local equivalence ratio of the fuel/air/oxidizer mixture should be between 0.2 and 2 [17]. Oxygen enrichment promotes ignition by providing a head start to the mixing process so that the required local equivalence ratio is reached sooner. Therefore, increasing the level of enrichment provides a greater head start.

Figure 13 shows a comparison between suppressed combustion and fuel into air with oxygen enrichment at EP = 13.9, i.e., the same fuel mass flow rate as the data shown in Figs. 9 and 12, but with approximately twice the amount of premixed oxygen as the data shown in Fig. 12. Doubling of the enrichment level has moved the position of ignition upstream to approximately $x = 750$ mm and has also moved the peak pressure rise of approximately 1.5 times the inflow pressure upstream to $x = 1000$ mm. The cycle analysis calculation shown for this data used a combustion efficiency curve shown in Fig. 10, which has an ignition point at $x = 750$ mm, a larger slope at the point of ignition than either of the earlier cases and a higher combustion efficiency at the end of the duct equal to $\eta_{c,e} = 60\%$. Doubling the premixing level has both further reduced ignition length and continued to increase the overall mixing and combustion level of the strut by an amount approximately equal to the level of premixing. Figure 14 shows enriched data at increasing

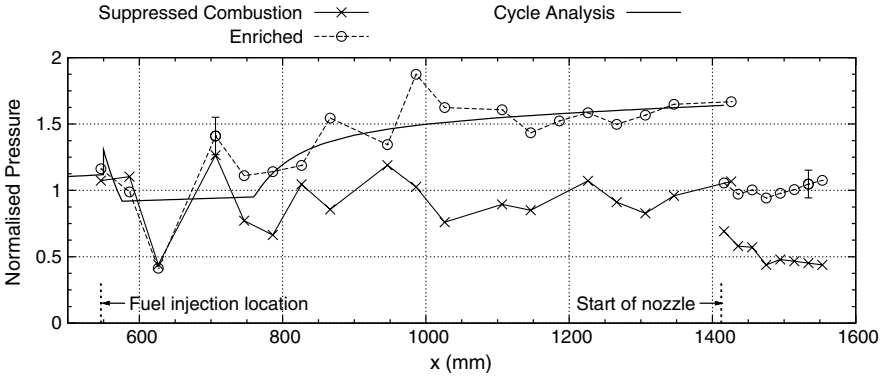

Fig. 13 Pressure distributions comparing enriched ($\phi = 0.81$, EP = 13.9) and suppressed combustion ($\phi = 0.85$, EP = 0).

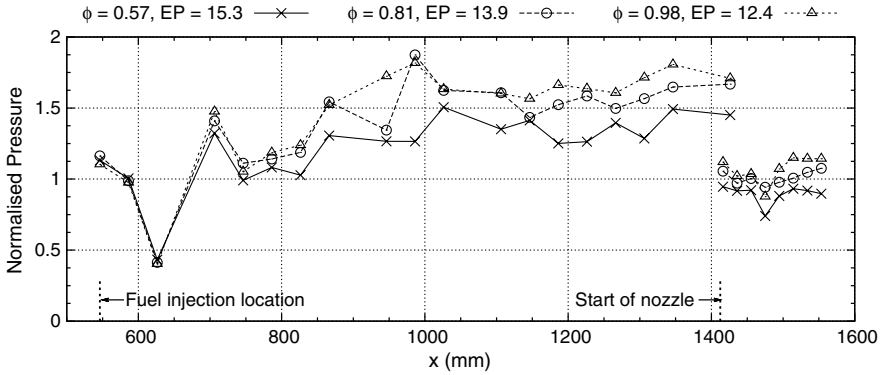

Fig. 14 Pressure distributions comparing fuel into air with enrichment experiments at increasing equivalence ratio.

equivalence ratio with approximately the same level of enrichment. The observed reduction in ignition length and upstream movement of the point at which the mixing limit of the strut is reached occurs for all equivalence ratios tested. The main effect of equivalence ratio is the same as for no enrichment: i.e., increased pressure rise at the end of the duct as ϕ is increased.

It has been noted that, in these experiments, combustion efficiency decreases with increasing fuel injection and is improved by the use of oxygen enrichment. These observations are summarized in Fig. 15, in which combustion efficiency for several experiments is plotted against the effective equivalence ratio. The use of ϕ_{eff} is more appropriate than ϕ in this instance since it is important to account for the premixed oxygen when drawing conclusions regarding combustion efficiency. In general, it has been shown that combustion efficiency decreases with increased equivalence ratio [19], which is seen as well for fuel-into-air experiments in Fig. 15. Oxygen enrichment reduces the effective equivalence ratio, so an increase in combustion efficiency could be attributed to the decrease in ϕ_{eff} and previously noted trends. However, there is in general an improvement in combustion efficiency for enriched experiments over fuel-into-air experiments at similar effective equivalence ratio. This is an indication that premixing allows for a larger percentage of fuel to burn to completion than would be possible without enrichment given the same ratio of fuel to oxygen in the duct.

From the presented data it is clear that oxygen enrichment reduces ignition length and increases the combustion efficiency of the current strut injector based combustor. It is of interest to examine the implications of these factors on the performance of a notional scramjet engine made up of the current constant-area combustor and a nozzle with an area ratio of 20. To analyze the performance of this engine, the 1-D properties calculated at the end of the constant-area duct were expanded to an area ratio of 20 assuming equilibrium chemistry and a loss coefficient of 0.9. Figure 16 shows the specific thrust generated by this configuration for both fuel into air and differing values of enrichment for a range of equivalence ratio. Since specific thrust is concerned with how efficiently the captured air is processed, the abscissa in Fig. 16 is ϕ, which accounts only for the captured air. With no enrichment, increasing the equivalence ratio raises the specific thrust in an approximately linear manner, as indicated by the least-squares linear fit in Fig. 16. The addition of oxygen increases the calculated specific thrust at all equivalence ratios by an amount which is roughly proportional to the level of enrichment. This is due to the increased combustion efficiency produced by enrichment at the end of the duct.

Also of interest to scramjet designers is the specific impulse, which is plotted in Fig. 17 for the notional scramjet described. The effective equivalence ratio is used here since specific impulse is a measure of how efficiently the propellant (i.e., fuel and premixed oxygen) is used. For the current experimental configuration, oxygen enrichment results in a $\sim$40% reduction in I_{sp}. This implies that there is potentially a significant mass penalty incurred from oxygen enrichment. However, when installed on a vehicle, it is highly likely that the improved specific thrust from oxygen enrichment could increase the net I_{sp}, i.e., when vehicle drag is taken into account.

More interesting plots are shown in Figs. 18 and 19, which present specific thrust and specific impulse estimates for a notional engine consisting of a combustor that is approximately half the length of the current duct ($L/h \sim 9$) and a nozzle expansion to an area ratio of 20. For this configuration, specific thrust levels for fuel into air with no enrichment increase linearly with ϕ, but at a smaller slope than the full length combustor configuration. This is because a combustor with $L/h \sim 9$ is too short for these hypervelocity conditions. For example, at $L/h \sim 9$ the combustion efficiency is only $\eta_c \sim 25\%$ for $\phi = 1.0$. Shortening the combustor does, however, decrease internal drag, which results in comparable specific thrust levels for both configurations. Conversely, halving the combustor length with

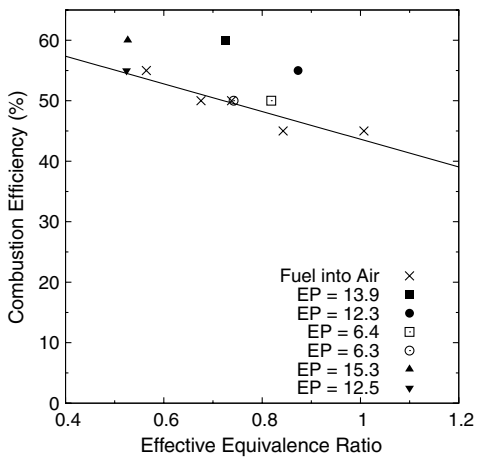

Fig. 15 Combustion efficiency estimates for fuel-into-air and enriched experiments.

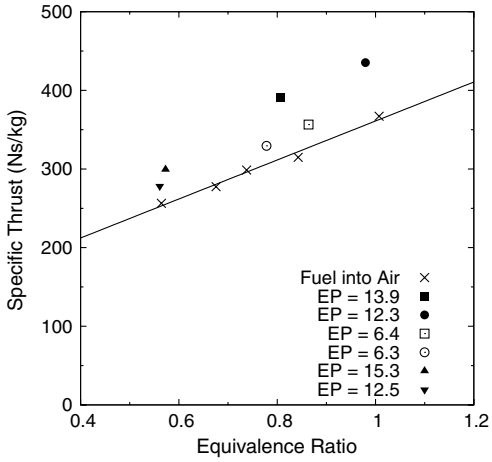

Fig. 16 Specific thrust estimates for a notional scramjet using the full duct length as a combustor.

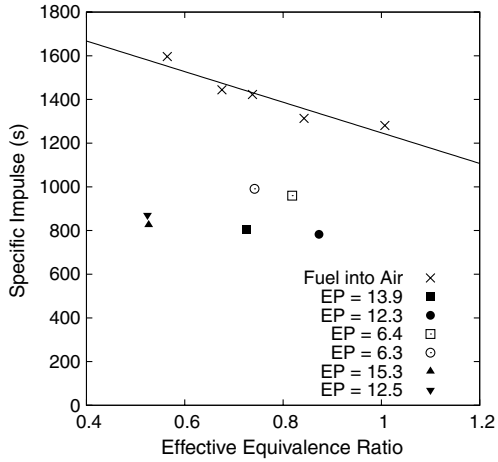

Fig. 17 Specific impulse estimates for a notional scramjet using the full duct length as a combustor.

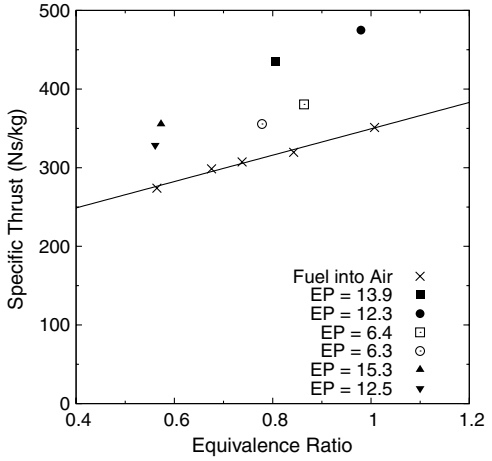

Fig. 18 Specific thrust estimates for a notional scramjet using approximately half the duct length as a combustor.

oxygen enrichment increases specific thrust slightly for all values of ϕ, as in most instances the combustion level is already close to its maximum at $L/h \sim 9$. This is due to the earlier ignition and larger slope in combustion efficiency upon ignition for enriched cases. At $L/h \sim 9$ and with $\phi = 1.0$, the combustion efficiency reaches $\eta_c \sim 50\%$ compared with $\eta_c \sim 25\%$ for no enrichment. As has been pointed out by numerous authors, scramjet combustor length must be

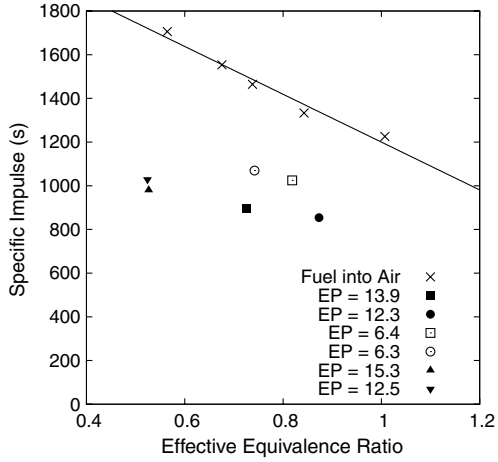

Fig. 19 Specific impulse estimates for a notional scramjet using approximately half the duct length as a combustor.

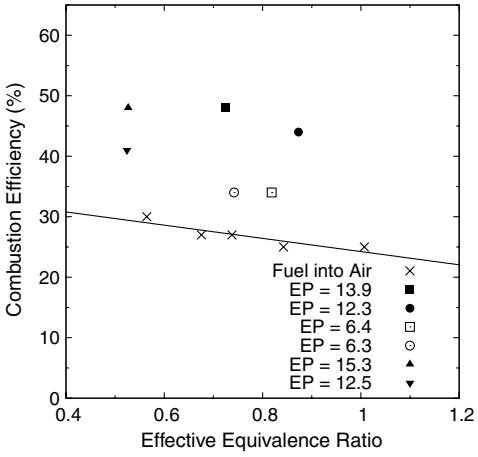

Fig. 20 Combustion efficiency estimates for a notional scramjet using approximately half the duct length as a combustor.

minimized, particularly at hypervelocity conditions, as drag and heat load in the combustor are extremely high [20]. With oxygen enrichment, shortening the current strut-based combustor results in greater specific thrust since drag is reduced and thrust is maintained at a high level.

Similar conclusions are drawn by examining the specific impulse. For fuel-into-air experiments, specific impulse decreases rapidly as ϕ_{eff} is increased since the combustor is too short to allow for much fuel to react. Conversely, for enriched experiments specific impulse is maintained at the same level as in the longer combustor since most of the fuel has reacted by $L/h \sim 9$. This is also reflected in the combustion efficiency at the end of the shortened combustor, which is plotted in Fig. 20 for comparison with Fig. 15. Enriched experiments with EP $\approx$ 12–15% are able to maintain combustion efficiency near the level attained in the longer combustor and are thus able to achieve high performance. Based on these results it is clear that oxygen enrichment shows the potential for significant scramjet performance improvement at hypervelocity conditions.

VII. Conclusions

Shock tunnel experiments were conducted to evaluate the effectiveness of oxygen enrichment at combustor conditions simulating flight at hypervelocity ($u > 3$ km/s, $M > 10$) in the atmosphere. Oxygen enrichment involves the premixing of oxygen with the fuel before injection into the engine combustor. It provides a head start for mixing and also allows the possibility of fuel combustion at greater than stoichiometric proportions. It is examined here as a means of extending scramjet operation to higher flight Mach numbers by increasing the specific thrust of the engine.

A generic, constant-area, rectangular combustor with a height of 47 mm and a length of 18.5 duct heights was used for the experiments. Gaseous hydrogen fuel, with and without oxygen enrichment, was injected along the axis of the combustor from a central strut injector, and pressure distributions were measured along the duct. The particular flight conditions simulated were a Mach number of 12.3 and a dynamic pressure of 40.2 kPa. These flight conditions were expected to result in poor mixing and combustion as a result of the high combustor flow velocity. Suppressed-combustion experiments, where fuel was injected into a nitrogen test gas, supplied the baseline results for the study. Fuel-into-air experiments at equivalence ratios up to one showed no difference compared with suppressed combustion until a distance of 350 mm (7.5 duct heights) downstream of injection. This was followed by a steady pressure rise until the end of the duct. Combustion was clearly mixing-limited in these experiments, and cycle analysis indicated a combustion efficiency of 45% for the maximum equivalence ratio of one.

Premixing of oxygen at levels that would burn with ~10% of the hydrogen fuel had two discernible effects. First, it reduced the ignition length by an amount approximately proportional to the

amount of enrichment. This was indicated by a pressure rise above the suppressed-combustion results upstream of that observed with no enrichment. Second, it increased the combustion efficiency at the end of the duct by an amount equivalent to the enrichment percentage. When considered as part of a notional scramjet made up of a combustor with half the current model duct length and a nozzle expansion to an area ratio of 20, these effects enabled an increasing level of specific thrust with increasing equivalence ratio, whereas no enrichment showed only marginally increased thrust with more fuel. The opportunity to retain a shorter combustor at hypervelocity flight is expected to be a key advantage of the technique.

These experiments, which are thought to be the first of their kind, show the positive effects of oxygen premixing with fuel in a scramjet combustor operating at hypervelocity conditions. Further experiments and analyses are required to determine if similar positive effects can be realized in complete scramjet flowpaths.

Acknowledgments

Financial support was provided by the Australian Research Council under grant DP0452374. S. A. Razzaqi thanks the T4 shock tunnel operators Wilson Chan, Rainer Kirchhartz, Andrew Ridings, and James Turner, as well as Keith Hitchcock, Milinda Suraweera, Tom Portwood, and Mark Bateup for their invaluable assistance during the experiments.

References

[1] Smart, M. K., and Tetlow, M. R., "Orbital Delivery of Small Payloads Using Hypersonic Airbreathing Propulsion," *Journal of Spacecraft and Rockets*, Vol. 46, No. 1, 2009, pp. 117–125. doi:10.2514/1.38784

[2] Kimura, T., and Sawada, K., "Three-Stage Launch System with Scramjets," *Journal of Spacecraft and Rockets*, Vol. 36, No. 5, 1999, pp. 675–680. doi:10.2514/2.3500

[3] Townend, L. H., "Domain of the Scramjet," *Journal of Propulsion and Power*, Vol. 17, No. 6, 2001, pp. 1205–1213. doi:10.2514/2.5865

[4] Bogdanoff, D. W., "Advanced Injection and Mixing Techniques for Scramjet Combustors," *Journal of Propulsion and Power*, Vol. 10, No. 2, 1994, pp. 183–190. doi:10.2514/3.23728

[5] Gardner, A. D., Paull, A., and McIntyre, T. J., "Upstream Porthole Injection in a 2-D Scramjet Model," *Shock Waves*, Vol. 11, No. 5, 2002, pp. 369–375. doi:10.1007/s001930200120

[6] Turner, J., and Smart, M. K., "Application of Inlet Injection to a Three-Dimensional Scramjet at Mach 8," *AIAA Journal*, Vol. 48, No. 4, 2010, pp. 829–838. doi:10.2514/1.J050052

[7] Rudakov, A. S., and Krjutchenko, V. V., "Additional Fuel Component Application for Hydrogen Scram-Jet Boosting," *SAE Aerospace Atlantic Conference & Exposition*, Dayton, OH, April 1990.

[8] Pike, J., "The Choice of Propellants: A Similarity Analysis of Scramjet Second Stages," *Philosophical Transactions of the Royal Society of London, Series A: Mathematical and Physical Sciences*, Vol. 357, 1999, pp. 2357–2378. doi:10.1098/rsta.1999.0435

[9] Ardema, M. D., Bowles, J. V., and Whittaker, T., "Near-Optimal Propulsion-System Operation for an Air-Breathing Launch Vehicle," *Journal of Spacecraft and Rockets*, Vol. 32, No. 6, 1995, pp. 951–956. doi:10.2514/3.26714

[10] Stalker, R. J., "Recent Developments with Free Piston Drivers," *17th International Symposium on Shock Waves and Shock Tubes*, edited by Y. W. Kim, Current Topics in Shock Waves, 1989, pp. 96–105.

[11] East, R. A., Stalker, R. J., and Baird, J. P., "Measurements of Heat Transfer to a Flat Plate in a Dissociated High-Enthalpy Laminar Air-Flow," *Journal of Fluid Mechanics*, Vol. 97, No. 4, 1980, pp. 673–699. doi:10.1017/S0022112080002753

[12] Paull, A., "A Simple Shock Tunnel Driver Gas Detector," *Shock Waves*, Vol. 6, No. 5, 1996, pp. 309–312. doi:10.1007/BF02535744

[13] Suraweera, M. V., and Smart, M. K., "Shock Tunnel Experiments with a Mach 12 REST Scramjet at Off-Design Conditions," *Journal of Propulsion and Power*, Vol. 25, No. 3, 2009, pp. 555–564. doi:10.2514/1.37946

[14] Portwood, T. W., "Enhancement of Hydrocarbon Supersonic Combustion by Radical Farming and Oxygen Enrichment," M.S. Thesis, Univ. of Queensland, Brisbane, Australia, 2006.

[15] Smart, M. K., "Scramjets," *The Aeronautical Journal*, Vol. 111, No. 1124, 2007, pp. 605–619.

[16] Shapiro, A. H., *The Dynamics and Thermodynamics of Compressible Fluid Flow*, Vol. 1, Wiley, New York, 1953.

[17] Heiser, W. H., and Pratt, D. T., *Hypersonic Airbreathing Propulsion*, AIAA Education Series, AIAA, Washington, D.C., 1994.

[18] Pergament, H. S., "Theoretical Analysis of Non-Equilibrium Hydrogen-Air Reactions in Flow Systems," AIAA-ASME Hypersonic Ramjet Conference, Paper 63113, 1963.

[19] Skinner, K. A., and Stalker, R. J., "Species Measurements in a Hypersonic, Hydrogen-Air Combustion Wake," *Combustion and Flame*, Vol. 106, No. 4, Sept. 1996, pp. 478–486. doi:10.1016/0010-2180(96)00018-1

[20] Paull, A., Stalker, R. J., and Mee, D. J., "Experiments on Supersonic Combustion Ramjet Propulsion in a Shock Tunnel," *Journal of Fluid Mechanics*, Vol. 296, 1995, pp. 159–183. doi:10.1017/S0022112095002096

N. Chokani
Associate Editor